Computational Methods for Localization

Fardad Askarzadeh,
CWINS, Worcester Polytechnic Institute, USA
faskarzadeh@wpi.edu

Yunxing Ye
CWINS, Worcester Polytechnic Institute, USA
yunxingye@wpi.edu

Umair I. Khan
CWINS, Worcester Polytechnic Institute, USA
uikhan@wpi.edu

Ferit Ozan Akgul
CWINS, Worcester Polytechnic Institute, USA
ferit@wpi.edu

Kaveh Pahlavan
CWINS, Worcester Polytechnic Institute, USA
kaveh@wpi.edu

Sergey N. Makarov
CWINS, Worcester Polytechnic Institute, USA
makarov@wpi.edu

Abstract

The concept of indoor localization has attracted considerable attention in the field of positioning. It has been reported that Time-Of-Arrival-based localization techniques exhibit superior performance relative to Received Signal Strength techniques or Direction-of-Arrival techniques. However, the accuracy of such systems is limited, mainly due to unexpectedly large ranging errors observed in indoor environments, caused by obstruction of the direct path by an object such as micro-metals and or a human body. The analysis of effects of the micro-metallic objects and human body on the accuracy of the range estimates are shown to be a very challenging problem. In this chapter we discuss the application of electromagnetic computational techniques to analyzing the effects of micro-metallic objects and the human body on the accuracy of range estimates. We use Finite Difference Time Domain (FDTD) direct solution to Maxwell's equations as well as Ray Tracing (RT) using Geometrical and Uniform Theory of Diffraction. The results of computational methods are compared to the channel profiles obtained from a real-time frequency-domain measurement to analyze the accuracy of the simulation methods.

Table of Contents

1. Importance of Channel Modeling

The effective design, assessment, and installation of a radio network require accurate characterization of the channel. The channel characteristics vary from one environment to another, and the particular characteristics determine the feasibility of using a proposed communication technique in a given operating environment. Having an accurate channel characterization for each frequency band, including key parameters and a detailed mathematical model of the channel, enables the designer or user of a wireless system to predict signal coverage, achievable data rate, and the specific performance attributes of alternative signaling and reception schemes. Channel models are also used to determine the optimum location for installation of antennas and to analyze interference between different systems.

The unpredictability of existing paths between transmitter and receiver in an indoor environment is very similar to the situation with outdoor channels, and in fact the work that has been done in characterization of mobile radio channels offers a useful guideline for modeling indoor channels. In an indoor environment, the multipath is caused by reflection from the walls, ceiling, floor, and objects within an office; in outdoor radio channels, multipath is caused by reflections from the ground as well as the buildings and vehicles in the vicinity of the mobile terminal.

There are two basic approaches to simulating wideband radio propagation characteristics: (1) measurement-based statistical modeling and (2) direct analytical solution of the radio propagation equations (computational techniques). Measurement-based statistical models are based on a mathematical description using several parameters. The parameter values are evaluated for each individual measurement of the wideband channel characteristics, and the statistics of the parameters over a large database are used to complete the model for a given coverage area. Statistics gathered from measurements in typical areas are extended to develop a more generalized model for all coverage areas. Statistical models generally do not incorporate details of the buildings in an outdoor coverage area or the layout of rooms within a building. Instead they classify all areas into a limited number of broadly designated environments and all buildings into a few classes of buildings.

In modem performance evaluations, the system designer is usually concerned with the overall performance over typical areas or typical buildings, and statistical models usually serve the purpose reasonably well. In other applications such as microcellular or indoor installations, where proper sitting of antennas is an important issue, building-specific radio propagation models offer a more precise tool for determining optimum antenna locations. Building-specific radio propagation models are based on direct solution of the radio propagation equations with boundaries defined by a map of a coverage area or the layout plan of a building. The technique known as *ray tracing* provides a simple approximation for analysis of radio wave propagation. Another approach is numerical solution of the Maxwell equations using the *finite-difference time-domain* (FDTD) technique. Ray tracing algorithms are also very useful for analysis of the angle of arrival of the paths for MIMO applications and the Time of Arrival (TOA) of the direct Line of Sight (LOS) path needed for the popular TOA based geolocation systems.

To compare the results of various computer simulation techniques, several approaches might be adopted. The most obvious approach is to compare the measured and simulated channel responses in typical locations. This method is not well suited for the evaluation of statistical models, because statistical models do not relate the channel response to a specific location. However, for assessing building-specific radio propagation models, this method is very useful. Another approach to evaluating the results of a simulation method is to compare empirical data with the cumulative distribution functions (CDFs) of the rms delay spread and multipath power produced by the simulation. Yet another approach for comparing radio propagation models is to evaluate the performance of a particular modem over the measured and modeled channels. Standard modulation techniques such as BPSK and wideband techniques such as

direct-sequence spread-spectrum or non-spread signaling with adaptive equalization can be used as benchmarks in these evaluation approaches.

The 2D ray tracing simulation technique was originally developed to analyze the behavior of wireless channels in small indoor areas using the two dimensional reflection and transmission model to trace rays by means of the ray shooting technique [1]. This model offered a low-cost means of propagation analysis for small indoor areas used for wireless local area network (WLAN) applications. Diffraction did not play a major role in most indoor radio propagation scenarios since the diffraction effect would influence propagation significantly only in locations such as corridors when the LOS path is blocked and the received signal involves multiple reflections and transmissions. However, this is not a likely situation for indoor WLAN applications, where terminals are typically used in reasonably open work areas.

Later, a 3D ray tracing simulation based on a typical residential area was developed to again analyze the behavior of wireless channel in macrocellular high-rise urban canyons with antennas installed above roof level. This simulation was based on the model that reflections and sharp edge diffraction were the main mechanism for simulation of signal propagation.

Although ray-tracing models can efficiently predict radio propagation characteristics for indoor and outdoor applications, these techniques are only approximations to the direct solution of electromagnetic wave propagation equations. The ideal method of simulating radio propagation is to solve Maxwell's equations numerically. The numerical solution of these differential equations over a designated area requires selection of a number of points at which the solution is to be determined iteratively.

The FDTD method is probably the most straightforward and widely used method for numerical solution of Maxwell's equations. With this method, Maxwell's equations are approximated by a set of finite-difference equations. By placing the electric and magnetic fields on a staggered grid and defining appropriate initial conditions, the FDTD algorithm employs the central differences to approximate both spatial and temporal derivatives, and it solves Maxwell's equations directly. The distribution of electric and magnetic fields over the whole grid is calculated incrementally in time; and when the simulation is finished, the propagation characteristics are known at every location in the area under study.

A more computationally efficient form of traditional FDTD method (for communication application) has also been applied previously to indoor areas, showing significant improvement in accuracy over the rectangular FDTD algorithm. The computational time needed for this method was comparable to that of a three-dimensional ray-tracing algorithm. A point-to-point comparison between predicted and measured power in all locations for two-dimensional and three-dimensional ray-tracing and for the FDTD models showed that both ray-tracing models and the FDTD model were all in good agreement with the measurements. However, ray-tracing provides a more accurate estimate of the power based on the standard deviation calculated against the measurements [1].

In general, the indoor localization problem is considered a challenging and difficult problem to formulate and model due mainly to the ever-changing characteristics of the wireless channel [1]. Results of a multitude of research studies have reported that time-of-arrival (TOA)-based techniques exhibit superior performance in line-of-sight (LOS) conditions when compared with received signal strength (RSS) and Direction-of-arrival (DOA) techniques [3][4][5]. This is due to the fact that location bearing metrics obtained from LOS measurement are more accurate than RSS and DOA metrics. The TOA of the direct path can then be related to the separation of the antenna pair. In 2-D scenarios three accurate distance measurements from known reference points (RPs) are enough to precisely determine the location of the mobile terminal.

However, the accuracy of the TOA-based technique degrades drastically when LOS conditions are not met [6][7], as confirmed in various measurement campaigns [2][8][22][23]. In such scenarios, mitigation of the ranging error plays a vital role in improving the accuracy of the system. This necessitates the use of modeling and estimation of ranging error in non-line-of-sight (NLOS) conditions. The first natural solution is the use of existing multipath models developed for telecommunication applications. However, these multipath models are based mainly on the delay spread of the channel and have not paid specific attention to the arrival time of the direct path. In all these models the first path is assumed to be the direct path. This assumption neglects the existence of the Undetected Direct Path conditions, which are one of the major causes of unpredicted large errors in TOA-based positioning systems,; we will discuss this in greater detail in the next section.

In the following sections, we introduce important parameters used in modeling a wireless channel. We provide a brief tutorial on the TOA-based technique and discuss challenges presented by that technique. We will also touch on measurement and simulation technique related to the TOA based technique.

2. Important Channel Model Parameters for Localization

Measurement and modeling of radio propagation for high speed wireless communications and localization is a challenging field of science and engineering. This is due to the fact that the radio channel suffers from temporal, spatial and direction of arrival fading caused by very complex random variations of the multipath components carrying radio signal from one location to another. In statistical measurement and modeling of the radio propagation, the radio channel between a wireless transmitter and receiver can be described by

$$h(d,t,\beta,\phi,\tau,\theta)=\sum_{i=1}^{L}\beta_i^d(t)e^{j\phi_i^d(t)}\delta[\tau-\tau_i^d(t)]\delta[\theta-\theta_i^d(t)] \quad (1)$$

where $h(d,t,\beta,\phi,\tau,\theta)$ is the overall channel impulse response at time t between the transmitter and receiver, which are at distance d from one another; and β,ϕ,τ, and θ are the amplitude, phase, delay of arrival, and angle of arrival of multiple arrivals paths of the transmitted signal. Since in wireless applications either terminal can be mobile or people may move around or between transmitter and receiver, these paths and the channel impulse response are also function of time and space. Using (1), the average received power for a given distance between the transmitter and the receiver corresponds to [1]:

$$P_d=\sum_{i=1}^{L}\overline{|\beta_i^d(t)|^2} \quad (2)$$

Here, the received signal power is the sum of squares of all path amplitudes. In the case of narrowband signaling [1],

$$P_d=|\sum_{i=1}^{L}\beta_i^d(t)e^{j\phi_i^d(t)}|^2 \quad (3)$$

where the amplitudes added vectorially and the overall power was the square of the resulting vector. As a result, the normalized received power of a narrowband signal is less than or equal to that of a wideband signal.

To calculate the distance between the transmitter and the receiver, we use the average RSS and a distance-power relationship to determine $\hat{d}$. If we define the distance measurement error as the difference between the measured and actual values of distance, $\varepsilon_d=\hat{d}-d$, this error in RSS systems would be independent of the bandwidth of the system. The power is calculated by a common principle behind all statistical models for the calculation of RSS that corresponds to:

$$RSS_d=10\log_{10}P_r=10\log_{10}P_t-10\alpha\log_{10}d+X \quad (4)$$

In this model, called the lognormal model, P_t is the transmitted power, d is the distance between the transmitter and the receiver, and α is the distance-power gradient of the environment. The random variable X is a lognormal distributed random variable representing shadowing effects.

In the case of propagation around a human body, environmental variations and body movements will cause path loss to be different from the mean value for a given distance. This phenomenon is called shadowing, and it represents the path loss variation around the mean.

In TOA systems, TOA measurement requires more complex receivers, and measurement accuracy depends on system bandwidth. A TOA sensor estimates the distance from $\hat{d}_w = c\hat{\tau}_{1,w}$, where c is the speed of light and $\tau_{1,w}$ is an estimate of the TOA of the direct path. Estimates of TOA are obtained by detecting the first peak of the received signal, and this value is a function of bandwidth and the occurrence of UDP conditions. The distance error is defined as

$$\varepsilon_{d,w} = \hat{d}_w - d \tag{5}$$

where d is the actual distance between the sensor and target object. In the next section of this chapter, where we focus on the TOA-based technique, the ranging error that is discussed in sub-section 3.1 and shown in Figure -2 are based on (5). The first statistical model for the behavior of TOA sensors in indoor area is a primitive model reported in [28]. This model uses the results of measurement-calibrated ray-tracing software to develop a statistical model for the distance measurement error and to relate that to the bandwidth of the sensor.

For communication applications, we need a convenient numerical measure of the time dispersion or multipath delay spread of the channel. A popular measure of delay spread is the root mean square (rms) delay spread, τ_{rms}, which is the second central moment of the channel impulse response. It is given mathematically by

$$\tau_{rms} = \sqrt{\overline{\tau^2} - (\overline{\tau})^2} \tag{6}$$

where, given L propagation paths,

$$\overline{\tau^n} = \frac{\sum_{i=1}^{L} \tau_i^n \mid \beta_i \mid^2}{\sum_{i=1}^{L} \mid \beta_i \mid^2} \tag{7}$$

These equations are the basis of delay spread calculations for the current 2D and 3D RT applications, discussed in later sections.

3. TOA Based Techniques

In the opening section of this chapter, we described the importance of channel modeling for localization purposes and explained how it differs from modeling a channel for communication purposes. Throughout the first two sections we refereed to multiple localization techniques and important channel parameters associated with each technique. We briefly touched on multiple measurement campaigns that had reported the TOA-based techniques showing superior results relative to RSS or DOA based techniques, when LOS conditions are present.

In this section we continue to address the TOA-based technique and discuss the challenges that arise with the use of TOA, by analyzing the behavior of its important channel parameters. We provide an extensive tutorial on measurement techniques and simulation procedures that are used to analyze the channel and understand its behavior in obstructed line of sight (OLOS) and undetected-direct-path (UDP) conditions.

Our overall objective in this section is to provide the reader with a good understanding of the TOA-based technique and its shortcomings for specific cases and an understanding of how researchers attempt to measure and simulate the channel behavior to predict ranging errors.

The details of TOA estimation techniques for wideband and ultra-wideband systems are discussed in the next part of this section titled as Challenges for TOA Techniques

3.1 Challenges for TOA techniques

The indoor radio channel suffers from severe multipath propagation and heavy shadow fading conditions so that measurements for localization are far from accurate in many instances. In general, measurements of Phase of Arrival (POA) and DOA in large indoor and urban areas provide very unreliable measurements. TOA and RSS estimation are also susceptible to large errors due to undesirable multipath conditions.. To accurately estimate TOA in indoor areas, we need to resort to different frequencies of operation and more complex signaling formats and signal processing techniques that can resolve the problems. The behavior of a TOA sensor in indoor multipath propagation is highly sensitive to the bandwidth of the sensor. The UWB systems, which exploit bandwidths in excess of 1GHz, have attracted considerable attentions as a means of measuring accurate TOA for indoor geolocation applications. However, as in other TOA systems, UWB systems cannot completely avoid UDP problems [21]. Figure 1 shows the basic concepts involved in wideband TOA measurements using the arrival time of the first path in a typical indoor multipath environment [22][23]. In this figure , the direct path (DP) is represented by the first path, which is also the strongest path. Location of this path is the expected value of the TOA. Other paths with a number of reflections and transitions arrive after the DP with lower amplitudes. These paths would have been observed at the receiver if the bandwidth of the system were infinite. In practice, bandwidth is limited, and the received signal comprise a number of pulses whose amplitudes and arrival times are the same as impulses but they are shaped pulse. The superposition of all these pulse shapes forms the received signal, which we refer to as the channel profile. A common practice is to estimate the location of the DP as the location of the peak of the first path that, is the estimated TOA. In a single path environment, the actual expected and the estimated direct paths are the same. In multipath conditions, however, as shown in Figure 1, the peak of the channel profile gets shifted from the expected TOA, resulting in a TOA estimation error caused by the multipath condition. We refer to the distance error caused by erroneous estimate of the TOA as the *distance measurement error,* which can be calculated using (5) as discussed in the previous section. For a given multipath condition we expect that as we increase the bandwidth the distance measurement error becomes smaller.

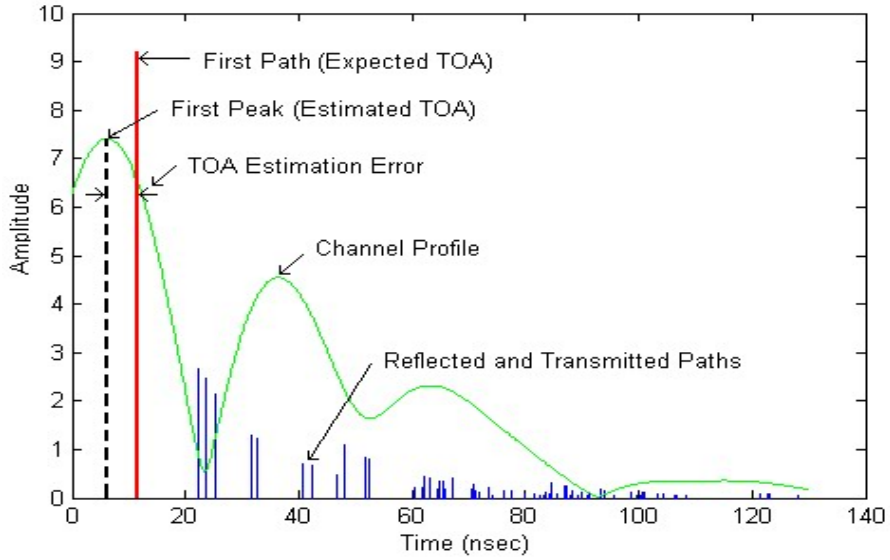

Figure 1: Parameters involved in wideband TOA measurement using arrival of the first path directly connecting the transmitter and the receiver

As a mobile terminal moves away from a base station the strength of the DP and the total received signal power decay exponentially. In an OLOS environment when the DP falls below the threshold while other paths are still detectable, the receiver assumes the first path in the profile to be the DP. This mis-identification causes a substantial error in wideband TOA measurements. We refer to this situation the UDP condition [21]. Figure 2 depicts the occurrence of the UDP scenario using the results of ray-tracing for a transmitted pulse with a bandwidth of 200MHz. Since the difference between the strength of the strongest path and the first path is more than the dynamic range (the range of detectable signal level below the strongest path) of the receiver, we have a clear UDP condition in which the first path is detected and declared as the DP resulting in a 5.23 m distance measurement error. With the release of UWB bands, the main challenge for the implementation of accurate wideband TOA systems is to find a remedy for UDP conditions.

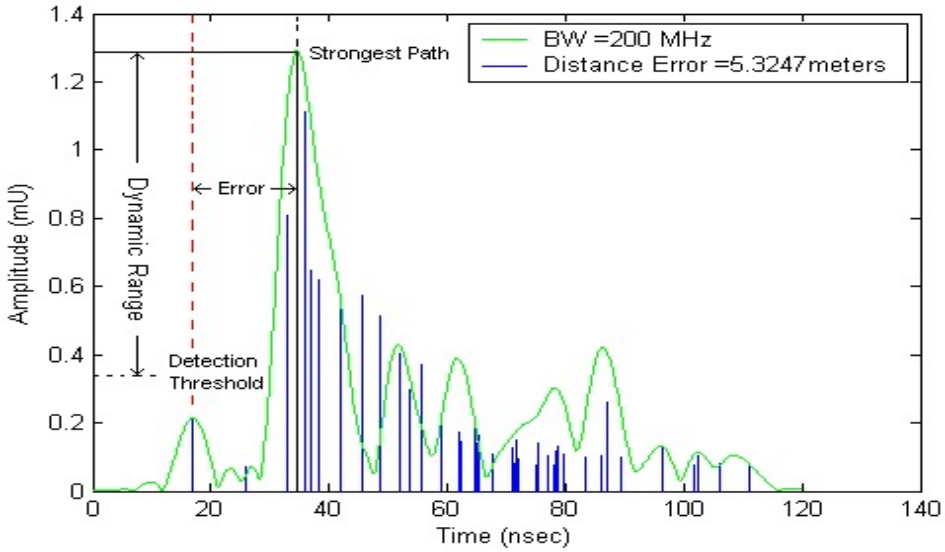

Figure 2: The UDP multipath condition from results of Ray tracing simulation and a channel profile with 200MHz

3.2 Simulation and Measurement Techniques

Considering the challenges to accurate localization discussed in the previous section, the most realistic approach to modeling the typical values of ranging error in such environments is to conduct empirical and statistical modeling , i. e., physical measurements [8][9]. However, conducting physical measurements can be time-consuming and tedious, which leads to a preference for the use of a controlled simulation environment. This allows the investigator to deal with a major problem, which is the effect of movements of objects and people in the area under study. Given the possibility of such movements, the environment is not controllable, thus preventing exact repetition of an experiment within the same environment. Therefore, researchers have recently examined a variety of computational methods for analysis of radio propagation pertinent to geolocation in multipath extensive areas.

The first approach to using a simulation environment for geolocation is to use RT software. Results of experiments reported in [2][8] illustrate that ranging estimates are greatly affected by the scattering objects (metallic objects or human bodies) around the transmitter and the receiver. As a result, it is difficult to associate the paths observed by measurements with those paths bounced from scattered objects, making it is extremely difficult to differentiate the effects of diffraction caused by micro-metal objects and human bodies from screening objects.

As discussed previously, the currently available indoor RT (2D) and FDTD applications were originally used to model indoor propagation scenarios. The delay spread of a wireless channel, described in (6) and (7), is important since TOA-based localization applications call for modeling of the direct path component, which is directly related to the ranging error. Therefore, this technique is inadequate for geolocation purposes.

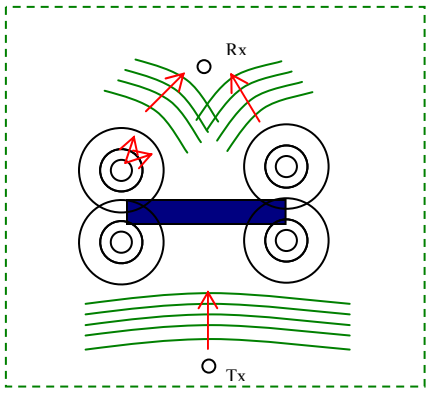

Figure 3 Diffraction around micro-metals (door)

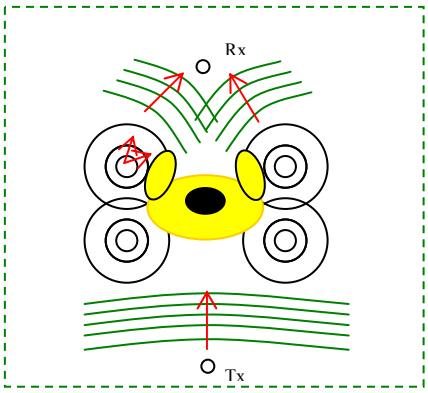

Figure 4 Diffraction around human body

As an example, in the past, a number of research projects have been carried out using one or more computational techniques to model Body Area Network channels. Among these, the most popular were FDTD, used by the National Institute of Standards and Technology (NIST) [17], and MoM used by the IEEE P802.15 working group [18]. Both these projects involved the modeling of the power delay profile of the human body channel for medical communication purposes, and not for TOA-based localization.

Lately the CWINS lab at Worcester Polytechnic Institute has been the pioneering the use of FDTD computational method for indoor geolocation purposes. In using FDTD simulation our aim is to overcome the challenges of TOA-based localization techniques by analyzing the effect of micro-metal objects [12] and the human body.

In the later sections, we will provide an overview of currently available simulation and measurement techniques for localization applications, their pros and cons and why we need the computational methods for indoor geolocation. For measurement technique, we will focus on the frequency domain measurement system for TOA based localization. For simulation techniques, we will introduce the Ray Tracing algorithm and the Finite Difference Time Domain method.

3.3 Channel measurement technology

In the early days of indoor wireless networking development, all wideband measurements were aimed at telecommunication applications, where the interests center mainly around signal coverage and rms delay spread analysis. The main objective of the indoor channel measurements is to establish a realistic foundation for the evaluation of indoor channel models. Measurements targeted for indoor geolocation application have been carried out in Center for Wireless information Networks (CWINS) since 1998 [28]. They were conducted primarily to study the distance measurement error behavior for different environment such as LOS, , OLOS, and UDP environments.

The most commonly used measurement technique for TOA-based localization is the use of the frequency-domain measurement system (Figure 5). The main component of this system is a network analyzer that sweeps the channel from 3 to 6GHz. After passing through a 30-dB amplifier, the output is connected to the transmitter antenna by a cable. The receiver is connected to an attenuator and then, through a low noise amplifier, to the receiver port of the network analyzer. The antennas are two UWB cone antennas. The analyzer has a sensitivity of -100dBm. The measurements are further calibrated to remove the effects

of the lossy cables, power amplifiers and other system imperfections. The measured frequency-domain data are passed through a Hanning window to further suppress the unwanted side lobes. Then the IFT is applied to estimate the time-domain channel profile. A threshold is used to characterize the channel profile according to the power of the direct LOS path. Estimating the time-domain power-delay profile requires estimating the relative amplitudes and delays of the arriving multipath components. Distinguishing between actual paths and measurement system noise required the implementation of a noise threshold. Since the noise floor of the measurement system is -100 dBm and the Hanning window has side lobes of -31dB relative to the peak of the profile, a threshold is selected according to the larger of the two values. Then, the first path having power greater than the noise threshold is the first detected path.

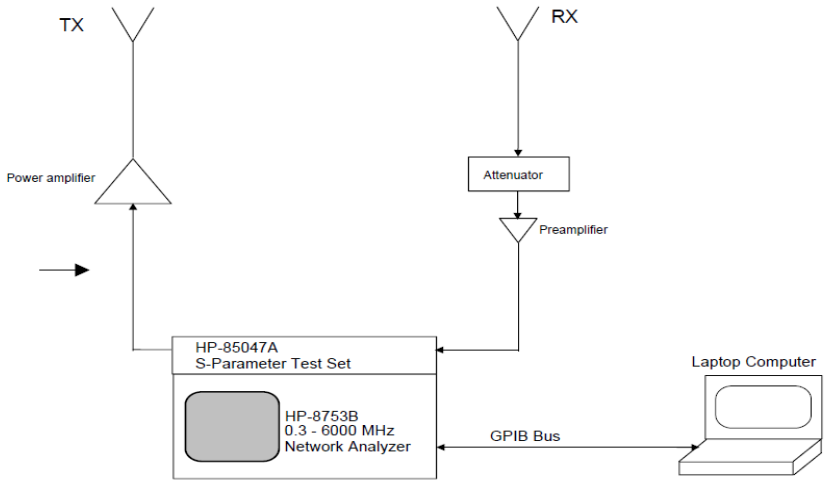

Figure 5: System for frequency domain channel measurement

3.4 Ray tracing algorithm

The Ray Tracing algorithm is an optimal tool for modeling radio propagation without incurring the labor cost of conducting empirical measurements. As a ray meets a wall, two paths emerge, one reflected and the other transmitted through the wall. There are two general approaches that can be employed to calculate these paths. The first uses optical images of the transmitter and receiver. In this approach, reflections of the transmitted signal by various reflecting objects in the floor plan are described by images of the transmitter, and these images are used with images of the receiver to find all the paths to the receiver. The second method for determining the reflected and transmitted paths is through the application of ray-shooting techniques. A pincushion of rays is sent out from the transmitter, and the progress of each ray is traced through the environment until the ray has either intersected the receiver or has lost enough power that its contribution to the received signal is negligible. The time of arrival, intensity, phase and direction of arrival are recorded for each ray that intersects the receiver. Once every ray has been traced to completion, the channel impulse response is formed. The user interface of a typical 2D RT software package is shown in Figure 6.

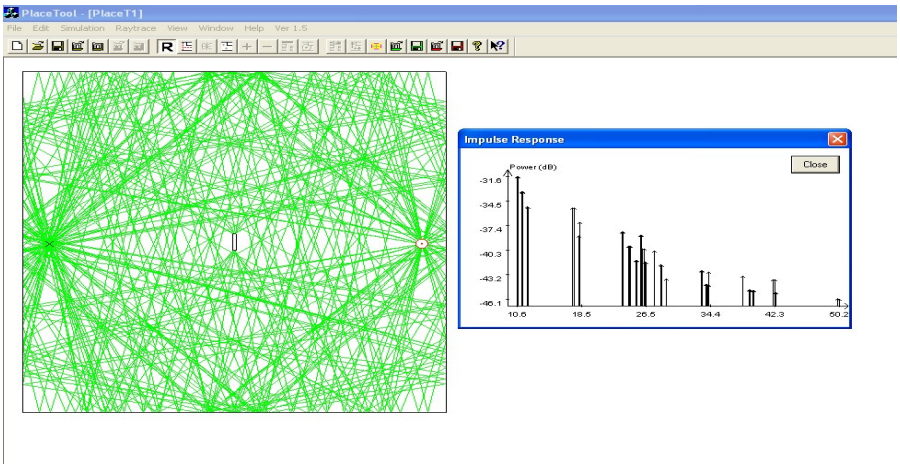

Figure 6: Typical user interface of a 2D Ray-Tracing software

The transmitter is represented by the red dot in the graph on the left screenshot in Figure 6, and the receiver is represented by the cross mark. The small bar in the center represents the overhead view of a metallic door. The channel impulse response is shown in the graph on the right screenshot. The same MATLAB code used to extract and process measurement data and is also used to process the RT simulation result. The dielectric constant of the walls and micro-metals in the graph can be adjusted to match the real environment. Since the effect of diffraction has not been included in the current RT software, the power of the direct path between the Tx and Rx would be significantly reduced by the metallic door. Therefore, when selecting the first path for ranging, we will mistakenly consider the reflected path from the outer walls as the direct path and thus suffer large positive ranging errors. Our simulation results confirmed this kind of error.

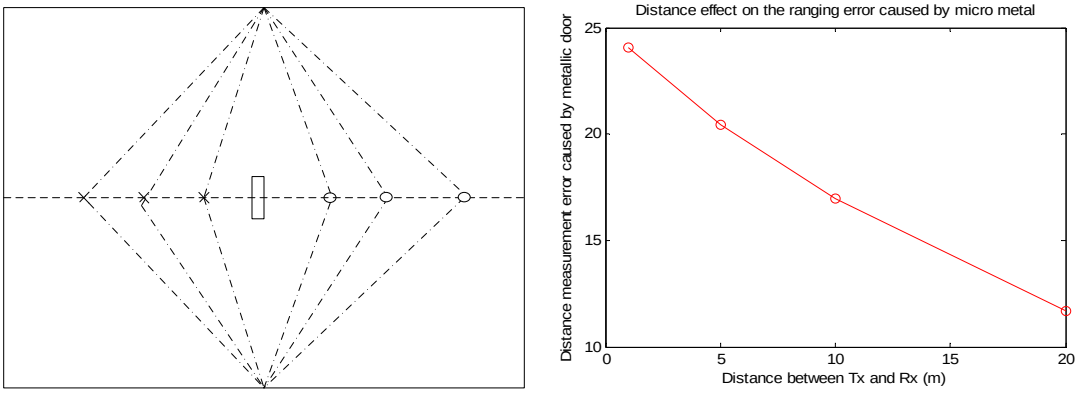

Figure 7: RT simulation senario and ranging error versus distance

As the distance between the Tx and Rx increases, the difference between the length of the direct path and reflected path decreases, hence the distance measurement error also decreases as we consider the reflected path as the direct path.

3.5 Finite-difference time-domain method

In 1966 Yee [1] proposed a technique to solve Maxwell's curl equations using the finite-difference time-domain (FDTD) technique. Yee's method has been used to solve numerous scattering problems for microwave circuits, dielectrics, and electromagnetic absorption in biological tissue at microwave frequencies. Since it is a time-domain method, solutions can cover a wide frequency range with a single simulation run. The FDTD method belongs to the general class of grid-based differential time-domain numerical modeling methods. The time-dependent Maxwell's equations are discretized using central-difference approximations to the space and time partial derivatives. The resulting finite-difference equations are solved in either software or hardware in a leapfrog manner: the electric field vector components in a volume of space are solved at a given instant in time; then the magnetic field vector components in the same spatial volume are solved at the next instant in time; and the process is repeated over and over again until the desired transient or steady-state electromagnetic field behavior is fully evolved.

Let us consider a two-dimensional *transverse magnetic* (TM)-to-z field (Electric and Magnetic fields are perpendicular to the Z-axis) as depicted in Figure 8. This figure presents a classic scattering/radiation problem where both the radiating and receiving antennas (dipole or monopole) are vertical. The TM to z field can be illustrated by Maxwell's equations, 8-10:

$$\frac{\partial E_z}{\partial t} = \frac{1}{\varepsilon}\frac{\partial H_y}{\partial x} - \frac{1}{\varepsilon}\frac{\partial H_x}{\partial y} - \frac{\sigma}{\varepsilon}E_z \qquad (8)$$

$$\frac{\partial H_x}{\partial t} = -\frac{1}{\mu}\frac{\partial E_z}{\partial y} - \frac{\sigma^*}{\mu}H_x \qquad (9)$$

$$\frac{\partial H_y}{\partial t} = \frac{1}{\mu}\frac{\partial E_z}{\partial x} - \frac{\sigma^*}{\mu}H_y \qquad (10)$$

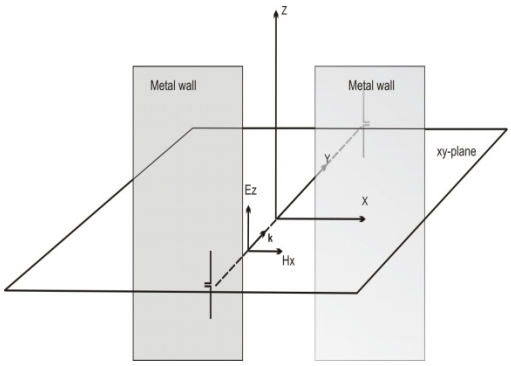

Figure 8: Two-dimensional traverse magnetic to Z-field

Here E and H are electric and magnetic fields, respectively; σ and σ^* are the electric and magnetic conductivities (losses), real or artificial. The standard Yee 2-2 FDTD scheme represented in (11) can be implemented [13] to operate on a staggered grid that is shown in Figure 9. In (11), E and H are discretized in time and space as the initial excitation travels through the computational area.

$$E_z(t,z)\to E_z\left((n-1)\cdot\Delta t,(k-1)\cdot\Delta x,(m-1)\cdot\Delta y\right)=E_{zk,m}^{n}$$
$$H_x(t,z)\to H_x\left(\left(n-\tfrac{1}{2}\right)\cdot\Delta t,(k-1)\cdot\Delta x,\left(m-\tfrac{1}{2}\right)\cdot\Delta y\right)=H_{xk,m+1/2}^{n+1/2} \qquad (11)$$
$$H_y(t,z)\to H_y\left(\left(n-\tfrac{1}{2}\right)\cdot\Delta t,\left(k-\tfrac{1}{2}\right)\cdot\Delta x,(m-1)\cdot\Delta y\right)=H_{yk+1/2m}^{n+1/2}$$
$$n=1,2,\ldots N_t-1 \quad k=1,2,\ldots N_x+1 \quad m=1,2,\ldots N_y+1$$

$$\frac{E_{zk,m}^{n+1}-E_{zk,m}^{n}}{\Delta t}=\frac{1}{\varepsilon_{k,m}}\frac{H_{yk+1/2,m}^{n+1/2}-H_{yk-1/2,m}^{n+1/2}}{\Delta x}-\frac{1}{\varepsilon_{k,m}}\frac{H_{xk,m+1/2}^{n+1/2}-H_{xk,m-1/2}^{n+1/2}}{\Delta y}-\frac{\sigma}{2\varepsilon_{k,m}}(E_{zk,m}^{n+1}+E_{zk,m}^{n}) \qquad (12)$$

$$\frac{H_{xk,m+1/2}^{n+3/2}-H_{xk,m+1/2}^{n+1/2}}{\Delta t}=-\frac{1}{\mu_{k,m+1/2}}\frac{E_{zk,m+1}^{n+1}-E_{zk,m}^{n+1}}{\Delta y}-\frac{\sigma^*}{2\mu_{k,m+1/2}}(H_{xk,m+1/2}^{n+3/2}+H_{xk,m+1/2}^{n+1/2}) \qquad (13)$$

$$\frac{H_{yk+1/2,m}^{n+3/2}-H_{yk+1/2,m}^{n+1/2}}{\Delta t}=+\frac{1}{\mu_{k+1/2,m}}\frac{E_{zk+1,m}^{n+1}-E_{zk,m}^{n+1}}{\Delta x}-\frac{\sigma^*}{2\mu_{k+1/2,m}}(H_{yk+1/2,m}^{n+3/2}+H_{yk+1/2,m}^{n+1/2}) \qquad (14)$$

In (11) , n represents the imaginary layer number that is calculated in the time domain and shown in Figure 9 as layer 0 and 1 (layers of electrical fields separated by Δt). The middle layer is represented as imaginary layer (n = 0.5). On the other hand, m and k represent the position of electrical or magnetic fields along the x or y axis of any of imaginary time domain layers. For example, (k = 1) represents the position of the second electrical field on (n = 0) layer from the t axis and (k = 0.5) represents the position of the first magnetic field on the (n = 0.5) layer from the t axis. Substitution of (11) into the fundamental Maxwell equations that are shown in (8)-(10) results in discrete formulas of ((12-14).

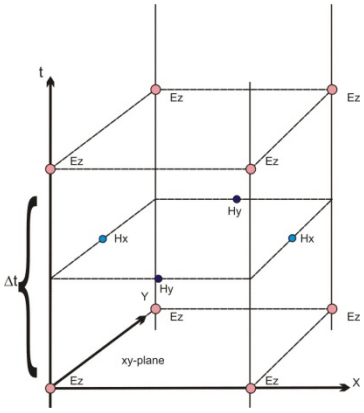

Figure 9 Scatter grids for the TM to Z mode

Formulas given in (12)-(14) are basically the core engine of any FDTD simulation software. Once we initialize the emanating electric and magnetic fields with the appropriate excitation values, a recursive call to these formulas, in time-domain, will predict electric and magnetic fields at any point within our computation space. From (12)-(14) we can clearly see that a 2D version of such a simulation would only calculate electric and magnetic fields for two specific dimensions. To better understand a 2D FDTD

simulation, one can visualize the simulation space as an imaginary plane. We can calculate fields, in time-domain, for any points located on this plane from the time an excitation emanates form the transmitter until it impinges upon the edges of the plane and the receiver point.

4. Computational Method and the Effect of Micro-Metals

Throughout the previous sections we explained how TOA-based techniques can suffer large ranging errors, mainly because of the effects of micro-metals and the human body around the transmitter and receiver. In this section, we focus on the effect of micro-metals and explain how a 2D FDTD simulation was used to precisely calculate the expected ranging error.

Around 2006 the CWINS lab at Worcester Polytechnic Institute launched a series of experiments to analyze and compare the results of TOA-based measurements with ray-tracing results. Measurements were made with the receiver placed behind a macro-metallic object (*i.e.,* metallic chamber in CWINS lab or the elevator along the corridor). The measurement results clearly exhibited a UDP condition due to the blocking of the first path [8].

The large discrepancy that was observed between ray-tracing and measurement results led the research team to examine the possible influences of micro-metallic objects such as doors or windows in those areas. Although introducing metallic objects to the ray-tracing map improved the discrepancies in some cases, it did not significantly affect the result of 2D ray-tracing.

To better understand the effects of micro-metals, a series of experiments was conducted to analyze and observe the behavior of the channel profile in close proximity to a metallic door. Figure 10 (left panel) provides the measurement results for each of three scenarios, which are depicted in the right panel of Figure 10. The blue graph indicates approximately 0.8 m Distance Measurement Error in close door scenarios as a result of diffraction of LOS due to closing the metallic door.

Considering the observed limitations of indoor RT simulation in the proximity of metallic objects, in order to analyze the effect of diffraction the research team initially decided to use Electromagnetic Computational Methods using Ansoft HFSS and CST FDTD simulation software. However, the extensive computational time required in using these packages led the group to use a custom MATLAB 2D FDTD software package, designed and developed for academic purposes, to expedite this process.

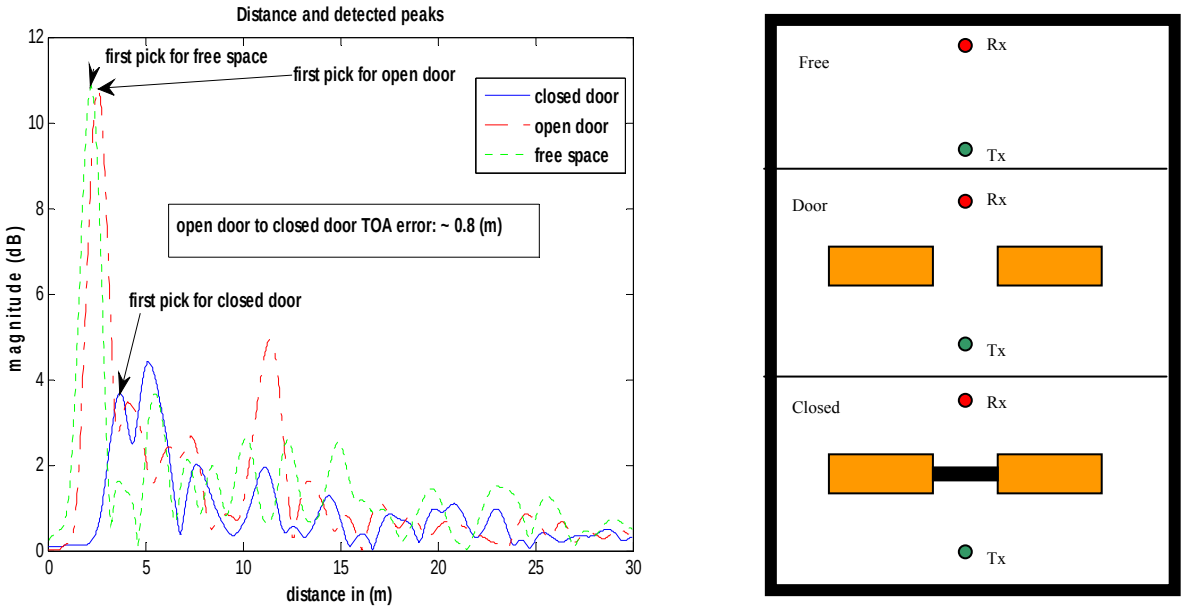

Figure 10. Measurement result for 2 m antenna separation.

(A) free-space (B) Open-door (door-frame) (C) closed-door

4.1. FDTD and the Effects of Micro-Metals

In the last subsection, we discussed the importance of the diffraction effect in proximity of micro-metals in indoor areas. In this subsection we provide a brief tutorial on this phenomenon.

When a propagating plane wave is incident upon a metallic-object such as a metallic door, that portion of the wave that impinges upon the edges is diffracted and continues traveling behind the object as a cylindrical wave. This diffraction phenomenon is shown in Figure 11(a), which schematically depicts a dipole antenna in close proximity to a metallic plane object, a metallic door.

At the same time, in terms of geometrical optics, which is used in ray tracing, the total field is considered to be a combination of rays emanating from the dipole and then reflected from the metal surface according to the Snell's law. According to geometrical optics, the field everywhere within the reflection boundary in Figure 11(b) is a combination of the incident (LOS) and the reflected signals. The field everywhere outside the reflection boundary, but still inside the shadow boundary, is the LOS signal from the dipole. The field below the shadow boundary is zero.

Ray tracing uses both diffraction theory and geometric optics, as we now explain. In the first half of the last century there was relatively little work being done on high frequency diffraction. However that changed in 1953 when Keller introduced the Geometrical Theory of Diffraction (GTD) as an extension of geometric optics to include diffracted rays [13]. This theory introduces diffracted rays in addition to the usual geometric optical rays used in Ray Tracing. Unlike in geometric optics, the diffracted rays can enter the shadow regions. This is a very important concept, because it makes it possible to calculate the high frequency radiation from antennas and scatterers of a quite general shape and to understand the various radiation mechanisms involved. Also, the GTD theory motivated the asymptotic treatment of the numerous canonical problems to determine the fields diffracted from edges, vertices and smooth curved surfaces [14].

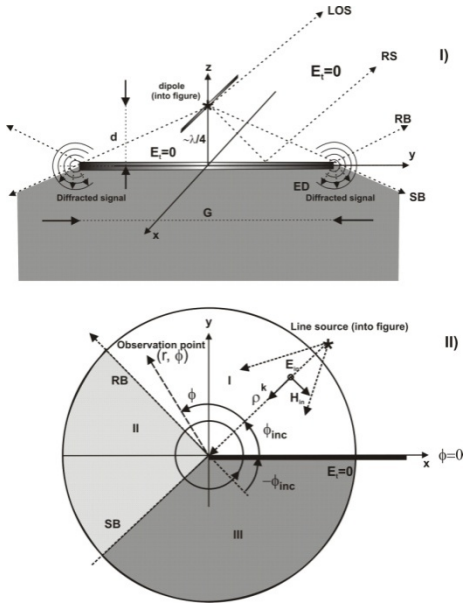

Figure 11. (a) Geometrical Optics approximation for dipole antenna Above a metallic plane ground (b) Problem formulization.

4.2 2D FDTD Simulation scenarios

Having outlined the theory of diffraction phenomena, we can now relate diffraction effect to each of the three scenarios depicted in Figure 10. In this part, we explain the simulation setup for each of those scenarios.

The very first scenario that we are going to discuss - which is the simplest one -is the free space scenario which, transmitter Tx and the receiver Rx are located 2 m away from each other without the effect of the environment (Figure 12 and 13).The other two scenarios are the ones that we are mainly interested in. There is either an aperture - a door opening in a metal screen, Figure 14 - or a metal scattered - a door in a dielectric screen - Figure 15. These figures present a two dimensional example with the Tx and Rx polarized in the direction that is perpendicular to the figure plane. In the open door scenario, the walls are simulated as dielectric material with ε_r = 12 approximately

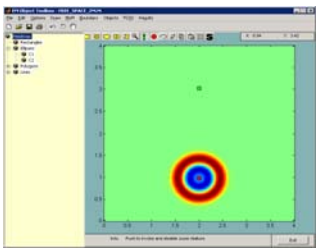

Figure 12 Free Space

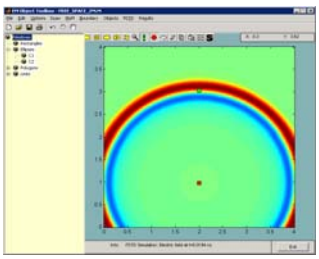

Figure 13 Free Space

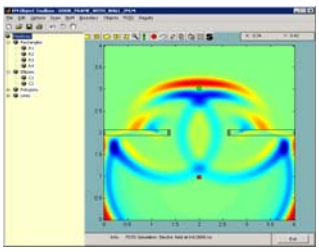

Figure 14 Open Door

and as shown in Figure 14, the signal emanates from the Tx in free space through the dielectric walls, and is received at the Rx in the presence of the door-frame. On the other hand Figure 15 clearly shows the penetration of waves through the walls and the diffractions phenomena that is experienced on the edges of the metallic door in closed door scenario.

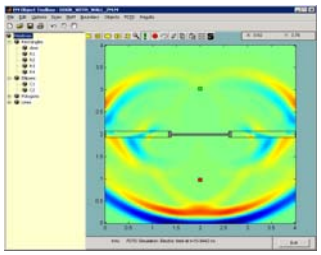

Figure 15 Closed Door

To set up our simulation environment, we configure the simulation area within relatively small dimensions of 4 m x 4 m with Perfectly Matching Layer (PML) walls surrounding the computational region and two antennas (a Transmitter and a Receiver) separated by 2m. The internal material of the box (2D square in our simulation case), are simulated as free space (μ_o, ε_o). To virtualize a door frame with two antennas on each side of it, we configure two walls with metallic sides away from each other by introducing an open space between transmitter and the receiver. The screening walls are simulated with dielectric constant of ($\varepsilon_r = 12$) and thickness of 12 cm. The metallic sides are provided with a thickness of 5 cm. The actual metallic door is simulated in dimensions of 1.21 m width and 44 mm thickness.

Figures 12-15 depict a snapshot of E-field wave propagation from the transmitter to the receiver antenna. In our simulation environment the small red square represents the transmitter (Tx) and the green square represents the receiver (Rx). A PML boundary is used to insure very little reflected energy from the truncated mesh. PML is a layer of artificial highly absorbing material surrounding the computational region. The PML is further terminated with Perfect Electric Conductor (PEC) surface.

4.3 Comparison of Computation with Empirical Results

The purpose in conducting a free-space scenario experiment is to prove the accuracy of our simulation result, while the open-door scenario serves to demonstrate how well the simulation approximates an ideal condition.

Through out Figures 16-17 emanating voltage time response is represented in red and the received voltage time response is represented in green. Using results derived from Figures 16 and 17, we see that the simulation provides us with a 1.99 m distance between the transmitter (Tx) and receiver (Rx) antennas. Comparing these results with the actual measurements that are derived from Figure 10-A shows that the simulation and measurement results are in good agreement. We can clearly see the effect of the environment in our measurement campaign (considering second and third picks, *etc.*), which are not captured in our simulation results due to the PML condition and the impulse signal nature of the transmitter in our simulation. Such a simulation is an ideal environment since the surrounding walls have little effect on our results.

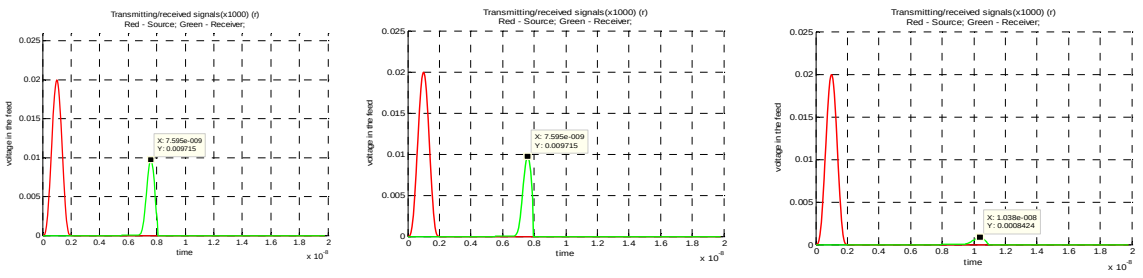

Figure 16 Free Space Figure 17 Open Door Figure 18 Closed Door

To simulate an open-door-frame scenario as shown in Figure 14, the setup was exactly the same as a free-space experiment except that we added a 2D representation of screening walls with a dielectric constant of $\varepsilon_r = 12$ and thickness of 12cm to our configuration. Part of this configuration was the design of the metallic door frame, which we simulated as metallic 2D rectangles with real dimensions of 5 cm widths. During the open-door experiment, we observed very close agreement between free-space simulation and measurement results.

Comparing Figures 16 and 18 we can conclude that the screening walls in the open-door scenario have no diffraction effect on the first path, which clearly reflects our measurement results shown in Figure 10 (left panel).

Figure 18 depicts the simulation result for the closed-door scenario. Using the result from Figure 18 we are able to calculate 2.81 m distance between transmitter (Tx) and receiver (Rx) antennas. Such a distance reflects a Distance Measurement Error of 0.81 m, which is close to what we see from the measurement as well. This DME is as a result of blocking of the first patch upon closing the metallic door. We also observe significant amount of signal attenuation, also due to conductivity of the metallic door.

4.4 Ray Optics and Effects of Micro-Metals

In the previous section we described how we used a custom 2D FDTD simulation to predict Distance Measurement Error in close proximity to a metallic door. The fact is that, since the custom 2D FDTD software was originally designed for academic purposes, it didn't completely fit to our experimental purposes. For that reason, we perused an alternative approach to 2D FDTD computational method by providing some enhancement to already available Ray Optics software.

Throughout this chapter we have noted at several points that the currently available indoor RT software routines not include diffraction, leaving this computational method inadequate to analyze the effect of diffraction in close proximity of metallic objects. For that reason we next discuss a new proposal offering an enhancement to currently available RT software, an enhancement enabling us to calculate the effects of diffraction in our simulations.

To better understand the proposed enhancement, consider Figure 19, which provides a comparison of the new proposed RT algorithm versus the current RT software that was developed for communication purposes. In a scenario where a metallic object is located between the transmitter and the receiver, the dashed red lines represent the behavior of current RT software in simulation of a cluster of rays emanating from Tx, interfacing with the metallic object and reflecting back, whereas they should be diffracted by the edges and received at the Rx point.

To conduct such a software enhancement, we introduce an analytical approach to Geometric Theory of Optics that can be added to the current indoor RT simulation. To do this, we take a rather different approach to analysis of diffraction by micro-metals by analytically calculating the power gain of diffraction rays around the edges of a metallic obstruction. We discuss a Geometrical and Uniform Theory of Diffraction method that uses an approximation to Kirchoff-Huygens function to analyze the effect of diffraction around the edges of micro-metallic objects that are obstructing a LOS path. The results of the GDT formula are compared with the channel profiles obtained from a real-time frequency-domain measurement in order to assess the accuracy of the formula calculation.

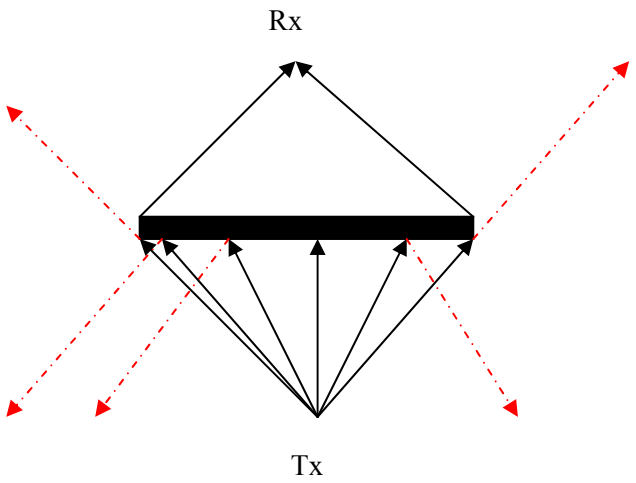

Figure 19 current available RT vs. RT with diffraction effect functionality

4.4.1 Analysis of diffraction around the edges

Figure 20 depicts a scenario in which a cluster of oblique plane waves is incident upon the edge of a metallic object. The rays that illuminate the edge in turn generate cylindrical waves that propagate behind the object.

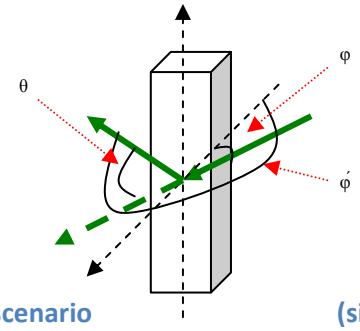

Figure 20: generic diffraction scenario (side view of two edge diffraction)

The Path Gain resulting from diffraction is given [15] by

$$PG = \frac{P_r}{P_t} = \left(\frac{\lambda}{4\pi}\right)^2 \frac{\left|D_{G0}(\theta)F(S)\right|^2}{\cos^2\psi} \frac{1}{rr_0(r+r_0)} \tag{15}$$

where θ is the angle of diffracted waves away from the edge (between the image of the incident wave and the diffracted wave), φ represents the angle between the incident wave and the perpendicular axis to the edge, and r_0 and r are the distances of Tx and Rx from the edge. The Diffraction coefficient function $D_{G0}(\theta)$ for a conducting screen is given by

$$D_{G0}(\theta) = \frac{-1}{\sqrt{2\pi k}}\left[\frac{1}{\cos(\frac{\varphi-\varphi'}{2})} + \frac{\Gamma_{E,H}}{\cos(\frac{\varphi+\varphi'}{2})}\right] \tag{16}$$

were, Γ_E = -1 for E parallel to the edge and Γ_H =1 for H parallel to the edge.

The transition (Fresnel) function $F(S)$, used to confirm the validity of GTD, is given by.

$$F(S) = 2j\sqrt{Se^{jS}} \int_{\sqrt{S}}^{\infty} e^{-ju^2} du \tag{17}$$

In (17), S varies based on the characteristic of the wave. For the cases that we are addressing here, diffraction of waves in contact with two edges, S can be defined as follows:

$$S = 2k\cos\psi \frac{rr_0}{r+r_0}\sin^2(\theta/2) \tag{18}$$

An approximation to $F(s)$ is given by

$$\sqrt{2\pi s}\left[f\left(\sqrt{2s\pi}\right) + jg\left(\sqrt{2s/\pi}\right)\right] \tag{19}$$

where

$$f(u) = \frac{1 + 0.926u}{2 + 1.792u + 3.104u} \tag{20}$$

$$g(u) = \frac{1}{2 + 4.14u + 3.492u^2 + 6.67u^3} \tag{21}$$

Figure 21 depicts the interaction of the incident waves with the edge of the door side, enabling a manual calculation of the Path Gain. In the figure, Tx and Rx are the transmitter and receiver.

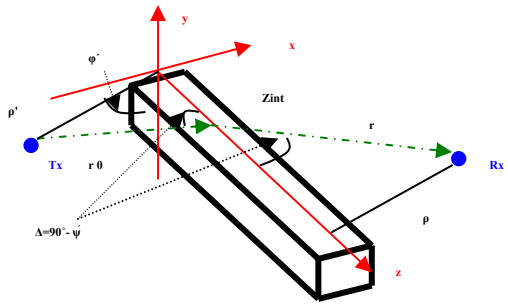

Figure 21: Abstract view of side edge diffraction of cabinet

There are also limitations to the manual calculation of the path gain introduced by diffraction. It is important to know that GTD is not valid near the shadow boundary where $\theta = 0$ and $D(\theta) = \infty$. More specifically, GTD is not valid in the transition region [16]. This means the antennas should be located $\pm\sqrt{\lambda x}$ away from edges where, x represent the distance of an antenna from the edge.

4.4.2 Comparison of Computation with Empirical Results

In order to calculate the power of waves diffracted from the edges of the micro-metallic door, we used the actual GTD formulas [16] to calculate the Path Gain. In order to verify the accuracy of the formulas, we will set up the same measurement scenario that was discussed in Figure 10.B .

For our experimental purposes, we used a custom antenna so that the propagated electric fields are parallel to the surface of the door, so that Γ_E = -1 in (16) for our analytical calculation.

The metallic door that we used in our measurements has dimensions of 201(cm) × 91(cm) × 4 (cm). The Tx and Rx are placed within 1 (m) of each side of the door. It is important to understand that, due to restrictions on GTD in transition regions as was discussed in previous section, the antennas should be placed about 3.45 (m) away from the doors

To conduct the experiment, a center frequency of 4.5 GHz was chosen, with 3 GHz signal bandwidth. The theoretical diffracted ray distance was calculated from the transmitter to one edge of the door, and from the edge to the receiver, which was 2.19 (m). While making the measurement, we recognized one of the

paths at this theoretical distance (among the paths that were not the strongest ones – in UDP condition) and measured its power. At this point we assumed this specific path to be the power of the signal diffracted from one edge of the door. Later, using an RF absorber, we attempted to block one side edge of the door, which abruptly caused a power reduction in the specific path. This experimental procedure led us to conclude that the path observed at ~2.2 (m) was a result of diffraction of rays around edges of metallic door.

As the next step of our experiment, we formulated (15)-(21) into a MATLAB code to calculate the path gain of diffracted waves from one edge of the metallic door for a bandwidth range of 1-5 GHz.

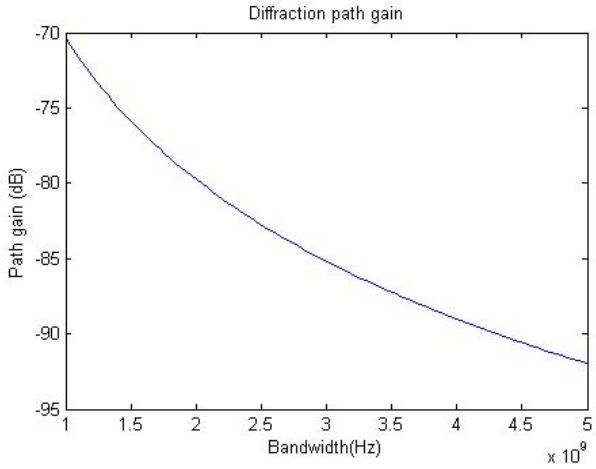

Figure 22 Path Gain (dB) Vs. Band Width (Hz)

As Figure 22 indicates, the calculated path gain is essentially reciprocal to the bandwidth of operation for a scenario in which antennas are placed 1(m) away from the surface of the metallic door. According to the analytical calculation, and as Figure 22 shows, the calculated Path Gain observed from one side edge of the door for 3 GHz bandwidth is approximately -85 dB.

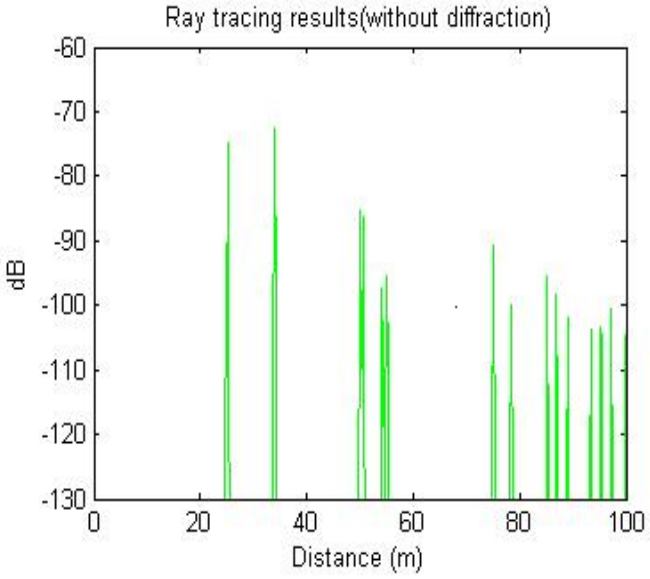

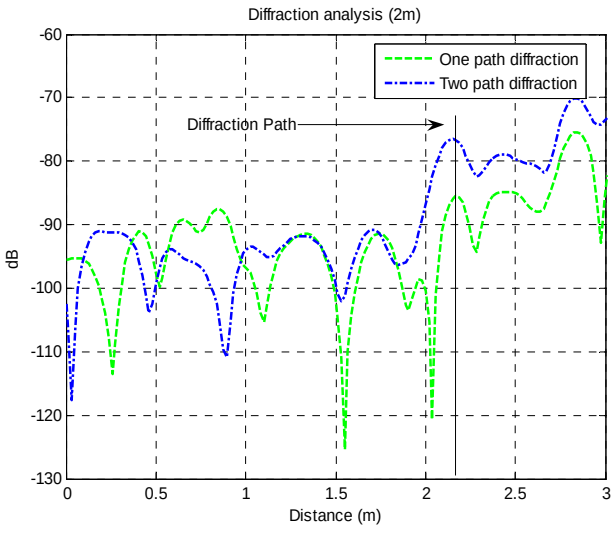

Figure 23 RT simulations for 2(m) antenna separation with metallic door in between

Figure 24 Measurement result for 2(m) antenna separation with metallic door in between

Figure 23 provides a snapshot of the RT simulation for a scenario in which antennas are in the proximity of 1 (m) from the surface of a metallic door. For comparison, Figure 24 shows the actual measurement result for the same scenario. The blue line represents the two-path diffraction from the edges of the door and the green line represents one-path diffraction. Comparing Figures.23 and 24 we can observe that the RT result provides approximately 25 (m) ranging error relative to the measured diffraction that is shown in blue and green in Figure 23.

Comparing the result of Figure 24 with the result of our analytical approach depicted in Figure 22 shows that the measurement results and the analytical results are in good agreement (PG = -85 dB),providing us a satisfying proof of concept for our proposed RT software enhancement.

5. FDTD and the Effects of the Human Body

In the past decade miniaturization and declining costs of semiconductor devices have allowed design of small, low-cost computing and wireless communication devices. These are used as sensors in a variety of popular wireless networking applications and this trend is expected to continue in the next two decades. One of the most promising areas of economic growth associated with this industry is being termed *wireless Body Area Networks* (BAN) or *Body Sensor Networks* (BSN). These networks are expected to connect wearable and implantable sensory nodes together and with the Internet as part of the emerging "Internet of Things" These networks will support numerous applications ranging from traditional externally mounted temperature meters or implanted pace makers to emerging blood pressure sensors, eye pressure sensors for glaucoma, and smart pills for precision drug delivery. A number of technical challenges regarding size and cost, energy requirements, and wireless communication technology are under investigation and at the core of these investigations is the importance of understanding radio propagation in and around the human body.

In January 2003, the Federal Communication Commission (FCC) defined a standard for medical implant communication, allowing two-way communication between implants in a frequency band at 402-405 MHz with a maximum signal bandwidth of 300 kHz. This band is called the *Medical Implant Communication Services* (MICS) band. The IEEE 802.15.6 Working Group was then formed to address standardization of these emerging technologies. As part of its deliberations, the IEEE 802.15.6 Working Group defines the technologies and models for characteristics of the medium for wearable and implanted sensor networks.
The human body is not an ideal medium for RF wave transmission. It is partially conductive and consists of materials of different dielectric constants, thickness, and characteristic impedance. Therefore, depending on the frequency of operation, the human body can exhibit high power absorption, central frequency shift, and radiation pattern disruption. The absorption effects vary in magnitude with both frequency of the applied field and the characteristics of the tissue. The shadowing should be considered for stationary and non-stationary position of body. Because of multipath reflections, the channel response of a BAN channel resembles a series of pulses. In practice the number of pulses that can be distinguished is very large and depends on the time resolution of the measurement system. The power delay profile of the channel is an average power of the signal as a function of the delay with respect to the first arrival path.

While channel models for communication sensor networks provide coverage and data rate limitations of sensor devices operating in specific frequencies allocated to the BANs, the models used in localization applications allow us to determine limits on precision of the location estimates for different implanted and body-mounted sensors. Localization for implant and body-mounted sensors is a new area of research that will draw on previous research at CWINS, WPI, ITS and NIST on indoor geolocation. Measurement of the radio characteristics for high speed wireless communications for BAN enables a number of applications mentioned earlier in this section. The measurement of localization characteristics of the BAN would enable another set of interesting applications for implant sensor localization for applications such as localization of wireless endoscopy equipment inside body and for body surface mounted applications, and localization of surgery equipment inside operation rooms. Innovations in wireless networks rely heavily on radio propagation measurement science and engineering in the specific environment and frequency of operation as well as bandwidth of the system. As a result, all wireless networking standardization committees devote substantial effort in measurement of the radio propagation characteristics to define channel models useful for performance evaluation of alternative wireless solution in a particular field of networking.

As discussed earlier, there are two ways a wireless channel can be modeled, either by direct measurements or by computational methods. The most popular way to study the characteristics of a channel is by first simulating a scenario in software using techniques such as Finite Difference Time Domain (FDTD), Method of Moments (MoM), Finite Element Method (FEM), Ray Tracing (RT), *etc*. and then comparing the results with actual measurements.

5.1 Measurement of Wideband Characteristics

As discussed earlier, the simplest way to model a channel is by taking actual measurements. Wideband measurements can be performed either in the time domain by direct measurement of the impulse response of the channel, or in the frequency domain by direct measurement of the frequency response of the channel. In theory, using Fourier transform techniques, the measured time and frequency responses should provide identical results. However there are some shortcomings in using the Fourier transform of the results of measurements, particularly if the measurement system does not provide both the magnitude and the phase of the measured characteristics [1].

The most intuitive measurement analysis for the human body would be to use people with different weights between the same transmitter and receiver. Figure 25 shows the measurement setup with a sample human subject of weight 156 lbs, which will also be used for the FDTD simulations in section 5.2. Figure 26 shows the impulse response of the channels with human subjects having different weights, each positioned between two 900 MHz dipoles. The bandwidth for this setup is 100 MHz. From Figure 26 we can see that as the weight increases, the first path power diminishes.

(a) (b)

Figure 25: Measurement setup (a) with body (b) without body.

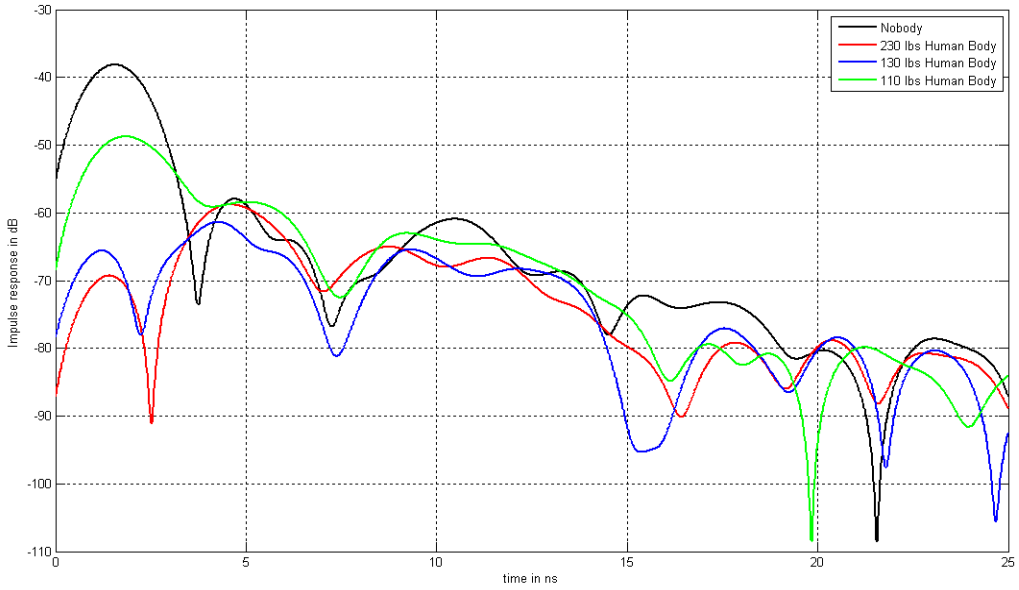

Figure 26 Impulse Response obtained from measurements with human subjects of different weights

Channel measurement and modeling for body surface mounted sensors is divided into Body-to-Body and Body-to-External experiments, which are further divided into LOS and Non-LOS (NLOS) scenarios. In LOS scenarios there is a direct unobstructed path between the transmitter and the receiver. In NLOS scenarios the body blocks the signal from direct connection path between the transmitter and the receiver. Figure 27 shows the results of two measurement experiments for body surface to body surface for LOS and body obstructed NLOS conditions, using Ultra Wideband (UWB) frequencies. In LOS experiments, we can clearly see the direct path which is also the strongest path. Considerable changes in multipath profiles suggest needs for separating LOS and NLOS channel models for these scenarios application.

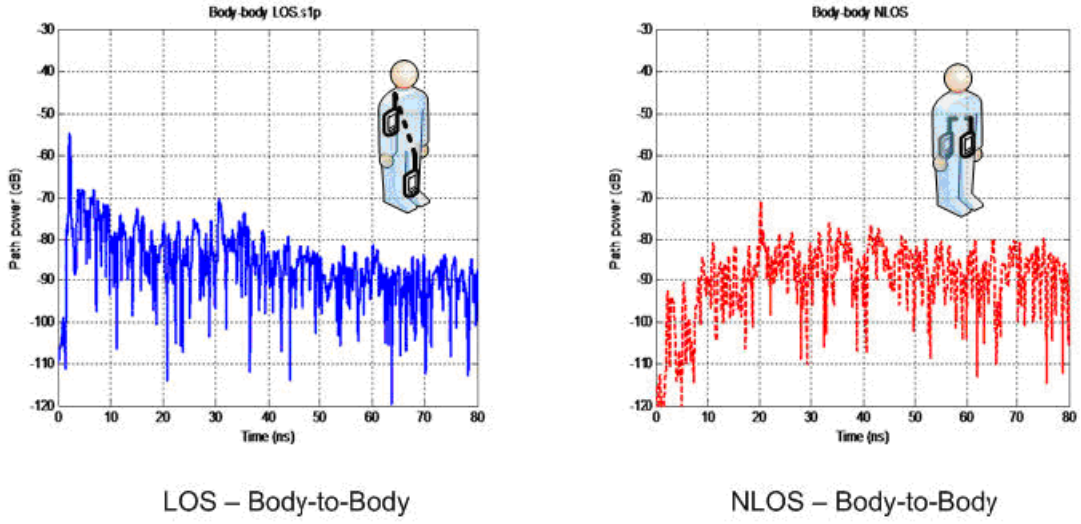

Figure 27: Channel impulse response in four different orientations of the body at Ultra Wideband (UWB) Frequencies

5.2 Computational Analysis of the Effects of the Human Body

Conducting physical measurements for localization can involve substantial effort to collect accurate databases for different environments of interest. This is more obvious in the case of the human body, where communication involving implants also has to be considered. In principle, employing computational methods does not require that any measurements be made; but some measurements are needed to check the accuracy of the computational methods and to determine the values of model parameters such as conductivity and permittivity of structural materials. The implementation of FDTD methods, however, always requires extensive computational resources.

Computation time for the FDTD technique is proportional to the size of the area, and the addition of structural details does not affect the computation significantly. However, the number of nodes used for computation is related exponentially to the size of the area and the frequency of operation. The computational methods can provide the relationship between the layout of a building or an outdoor area and the detailed channel response in a specific location. Therefore, they can provide realistic estimates of the azimuthal distribution of rays received in a multipath environment. In this section we discuss FDTD as a possible computational method to analyze the different characteristics of a channel.

5.2.1 An Overview of Ansoft HFSS

HFSS is a high-performance full-wave electromagnetic (EM) field simulator for arbitrary 3D volumetric passive device modeling that takes advantage of the familiar Microsoft Windows graphical user interface. It integrates simulation, visualization, solid modeling, and automation in an easy-to-learn environment where solutions to your 3D EM problems are quickly and accurately obtained. Ansoft HFSS basically employs the Finite Difference Time Domain (FDTD) methodology (that was described in sub-section 3.5 of this chapter), adaptive meshing, and brilliant graphics to give you unparalleled performance and insight to all of your 3D EM problems. Ansoft HFSS can be used to calculate parameters such as S-Parameters, Resonant Frequency, and Fields.

HFSS is an interactive simulation system whose basic mesh element is a tetrahedron. This allows you to solve any arbitrary 3D geometry, especially those with complex curves and shapes, in a fraction of the time it would take using other techniques. The name HFSS stands for High Frequency Structure Simulator. Ansoft pioneered the use of the Finite Difference Time Domain (FDTD) for EM simulation by developing/implementing technologies such as tangential vector finite elements, adaptive meshing, and Adaptive Lanczos-Pade Sweep (ALPS).

The human body model in HFSS has a millimeter level accuracy with 300+ objects including bones, muscle and organs. All frequency dependant material parameters are included. The following sections will show that the use of this software is a valid technique to analyze the multipath characteristics of the human body channel for wideband communication and TOA-based localization. Moreover, as already established in existing literature, we can also use it to analyze Received Signal Strength (RSS) based communication and studying path-loss models. Figure 28 (b) shows the electric field plot obtained from an HFSS ^{TM} simulation that will also be used to analyze the wideband characteristics of a wireless channel with a human body. This plot shows how the electric field, and hence normalized power, decays from the transmitter to the receiver.

5.2.2 Analysis of Path-Loss Models

A number of papers have been written using one or more if these techniques to model Body Area Network channels. The workgroup at National Institute of Standards and Technology (NIST) [17] used Ansoft HFSS™. They studied implant communications for medical purposes using the Medical Implant Communication Services (MICS) band with a range of 402-405 MHz. For this purpose they constructed an immersive 3D platform to better understand the EM propagation to and from the implants. Since their purpose was medical communication, they created a statistical path loss model including a random variable for shadow fading for deep tissue and surface tissue implants.

A more comprehensive study was done by the IEEE P802.15 workgroup [18]. This study included channel models for implant, as well as for surface communications. Furthermore, besides the MICS and UWB bands, the other bands used had center frequencies 600 MHz, 900 MHz and 2.4 GHz. However, contrary to [17], which used FEM simulations only; this study used measurement results as well as FDTD simulations using the SEMCAD ® software. The surface measurements were carried out on actual people and a phantom. These measurements used all the aforementioned frequency bands. The implant channel model was designed using the SEMCAD FDTD software and only used the MICS band. The purpose of this research was also medical communication; therefore not much priority was given to the multipath characteristics of the channel, except for UWB communications.

One of the initial works on the path loss models for body area networks was an electronic letter published by IEEE and submitted by the Department of Information Technology (INTEC) at Universiteit Gent, Belgium [19]. This work was also done for surface communications and used two software tools, FEKO ® for MoM and SEMCAD for FDTD simulations. In addition to these a rectangular phantom was also used for measurements. The frequency band used for this research was also 2.4 GHz. As implied earlier, the focus of this research was also a path-loss model for medical communication purposes, so the multipath characteristics of the channel were not examined.

Other research has also been done to plot the Specific Absorption Rate (SAR) of the human brain when a cellular antenna is placed near it, but they concentrate on only a very limited part of the human body and their purpose is only to make cellular technology biologically safer.

4.4.1 Experimental Procedure using the Ansoft HFSS suite

The research being carried out by the Center for Wireless Information Networks (CWINS) at Worcester Polytechnic Institute (WPI) is based on the application of localization and hence, the results are more concentrated towards the multipath characteristics of the channels. At the moment, only surface to surface measurements have been taken and have been compared with the FDTD simulation using Ansoft HFSS ™.

Both in the actual measurements and the software simulation, two dipoles in the 900 MHz band were placed 50 cm apart (Figure 25 (a)) and their S21 parameter was plotted over a bandwidth of 100 MHz. This plot was then used to find the impulse response using the chirp z-transform function in Matlab ™. After this a person with height 172 (cm) and weight 156 lbs was made to stand between the two antennas (Figure 25 (b)) and a human body model with similar characteristics was placed in the HFSS ™ simulation, between the two antennas (Figure 28). The impulse response for this new channel was also plotted much in the same way as before and the comparative results are shown in Figure 29. The side faces of the radiation box in the HFSS simulations were assigned concrete as their material and the front and back faces were assigned the radiation boundary to imitate the environment of the lab.

From the measurement taken without the body, the TOA of the first path was calculated to be 1.70 (ns), which roughly translates to about 51 (cm) - an error of 1 cm from the actual distance. The same value from the HFSS ™ simulation came out to be 1.95 (ns), which roughly translates to 58 (cm), indicating an

error of about 7 (cm) from the measurement. The TOA of the first path from measurements taken with the body came out to be 2.00 (ns), translating into 60 (cm), which means the human body added an error of 9 (cm) in the measurements. But the simulation with the body showed the TOA of the first path to be 1.70 (ns), again an error of 9 (cm) from the measurements but in the other direction.

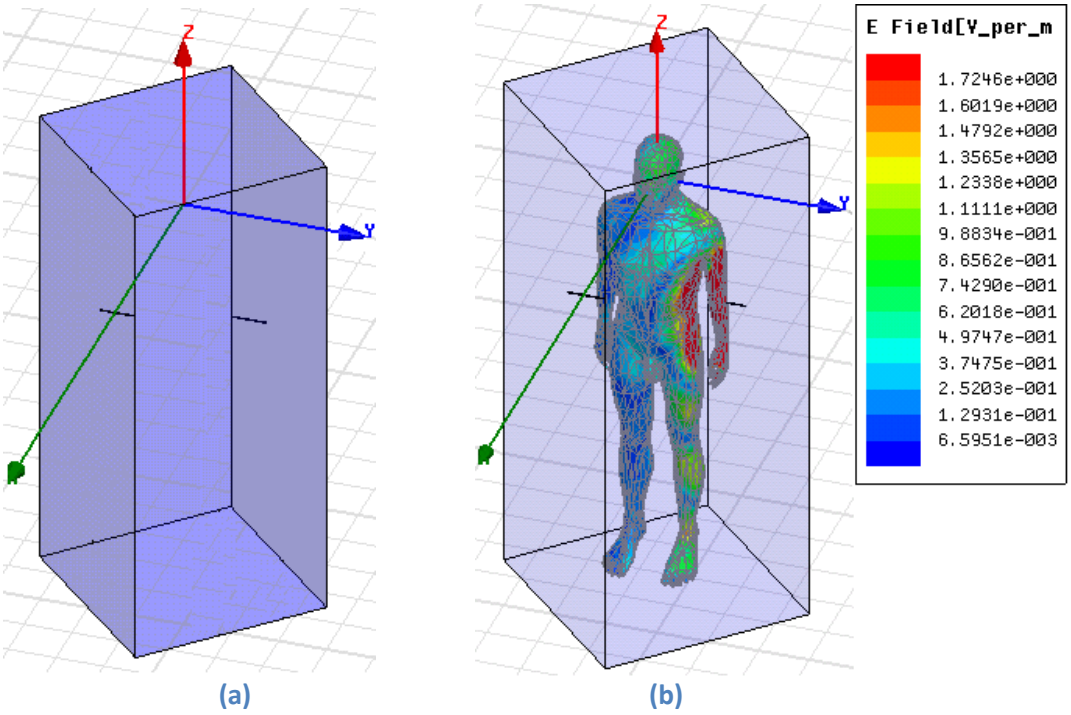

Figure 28 : Ansoft HFSS ™ simulation setup (a) without body (b) with body and electric field plot. The two horizontal black lines represent the dipoles.

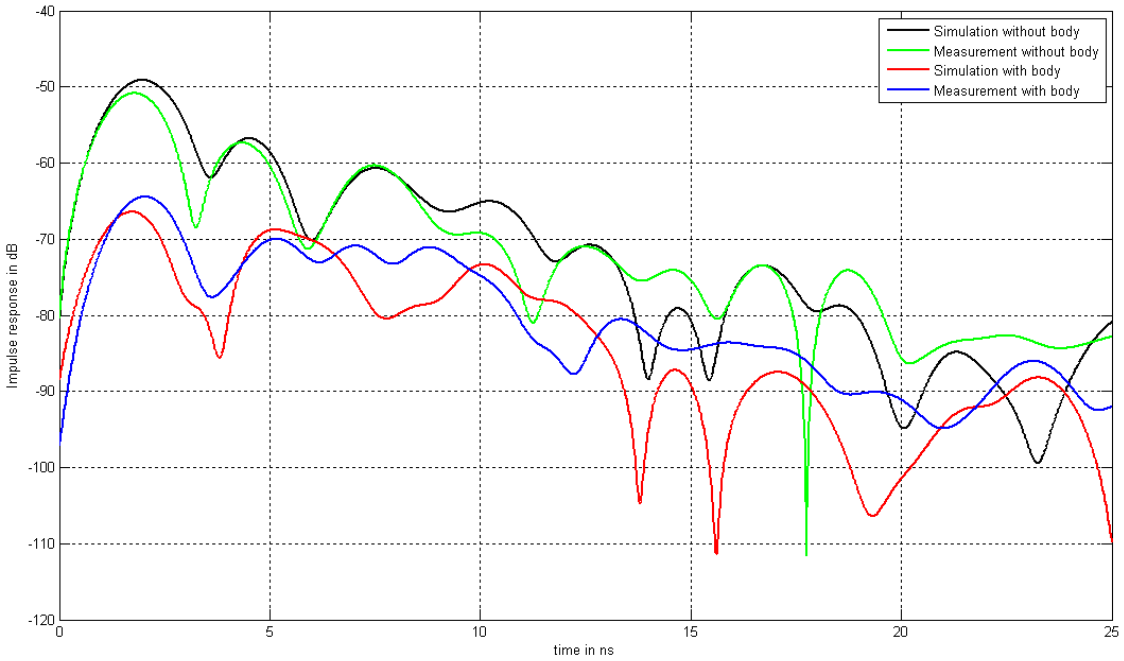

Figure 29: Impulse response obtained from the two simulated and measured channels

From Figure 29 and Equations (6) and (7), the rms delay spread of the first three paths for the measurements without the body came out to be 4.12 (ns) and that of the simulation without the body came out to be 3.97 (ns); a difference of just 0.15 (ns). When the body was added to the measurement setup, the rms delay spread was calculated to be 3.79 (ns), the same value for the simulation with the body came out to be 3.32 (ns); an error of about 0.47 (ns). Hence even the rms delay spread of the HFSS ^{TM} simulation was very close to that of the actual measurements, rendering little doubt that it is a valid mean to simulate the wideband profile of a channel.

As promising as these results seem, there is a need to continue with more measurements with absorbing boundaries. Also with the addition of a phantom, implant to implant measurements can also be taken and compared to their respective simulation results.

6. Conclusion:

In this chapter we provided an overview of the importance of channel modeling for indoor geolocation purposes and we discussed important parameters of a channel associated to each localization technique. We referred to multiple measurement campaigns which proved TOA-based technique performs superior to others techniques when LOS condition is met. This led us to focus our attention on TOA-based technique throughout this chapter and described the challenges that are involved with that.

We explored the applicability of computational method for TOA-based localization technique in close proximity of micro-metals and human bodies. We discussed that ray-tracing software can be considered as a computational method however; since the available indoor RT software had been designed for telecommunication purposes and dose not include diffraction leaves this technique inadequate to analyze the effect of diffraction. As a result, a 2D FDTD simulation software was used to analyze the effect of diffraction in close proximity of micro-metals. Although the 2D FDTD solver computationally tended to be a fast package but since it was originally developed for academic purposes, it did not completely fit our experimental purposes. This led us to consider an alternative approach of calculating the diffraction by proposing an enhancement to current Ray Optic software that included two-edge diffraction of micro-metallic objects.

Finally, we introduced HFSS, 3D FDTD software, to model the effects of the human body in close proximity to the transmitter and receiver antennas. We described the measurements taken around the human body as a yardstick to compare with the simulations. After this, we provided an overview of previous work done to model the path-loss characteristics of a wireless channel with the human body in between. Ultimately, we established that the FDTD software can be used to model wideband characteristics of the channel. We did this by taking measurements with the human body between the transmitter and receiver antennas, and then comparing these measurements with their HFSS simulation to get a good match.

Acknowledgements

We would like to thank Dr. Allen Levesque, Dr. Reza Zekavat and Dr. Mohammad Heidari for their invaluable suggestions and contributions. We are indebted to them for their technical support throughout this chapter.

References

[1] K. Pahlavan and A. H. Levesque, *Wireless Information Networks,* 2nd ed., New York: John Wiley and Sons, 2005.
[2] B. Alavi, "Distance Measurement Error Modeling for Time-of-Arrival Based Indoor Geolocation," Ph.D. Dissertation, Worcester Polytechnic Institute, 2006.
[3] H. Hatami and K. Pahlavan, "Performance Comparison of RSS and TOA Indoor Geolocation Based on UWB Measurement of Channel Characteristics," *IEEE Internation Symposium on Personal, Indoor and Mobile Radio Communications,* September, 2006.
[4] Catovic and Z. Sahinoglu, "The Cramer-Rao Bounds of Hybrid TOA/RSS and TDOA/RSS Location Estimation Schemese," *IEEE Communication Letters,* vol. 8, no. 10, pp 626-628, October, 2005.
[5] Y. Qi, H. Kobayashi, and H. Suda, "Cramer-Rao Bound for Geolocation in non-line-of-sight Environment," *IEEE Transactions on Wireless Communications,* vol. 5, no. 3, pp 672-681, March 2006.
[6] S. Gezici et al., "Localization via Ultra-Wideband Radios: A look at Positioning Aspects for Future Sensor Networks," *IEEE Signal Processing Magazine,* vol. 22, no. 4, pp 70-84, July 2005.
[7] H. Sayed, N. Tarighat, and N. Khajehnouri, "Network-Based Wireless Location: Challenges faced in Developing Techniques Accurate Wireless Location Information," *IEEE Signal Processing Magazine*, vol. 22, no. 4, pp 24-40, July 2005.
[8] N. Alsindi, X. Li, and K. Pahlavan, "Analysis of TOA Estimation using Wideband Measurements of Indoor Radio Propagations," *IEEE Transactions on Instrumentation and Measurement,* vol. 56, no. 5, pp 1537-1545, October 2007.
[9] S. Howard and K. Pahlavan, "Measurement and Analysis of the Indoor Radio Channel in the Frequency Domain," *IEEE Transactions on Instrumentation and Measurement,* vol. 39, no. 5, pp 751-755, October 1990
[10] T. Holt, K. Pahlavan, and J. F. Lee, "A Graphical Indoor Radio Channel Simulator using 2D Ray Tracing," *IEEE International Symposium on Personal, Indoor, and Mobile Radio Communications,* pp 411-416, October 1992
[11] G. Yang, K. Pahlavan, and J. F. Lee, "A 3D Propagation Model with Polarization Characteristics, in Indoor Radio Channel," *IEEE Global Telecommunication conference,* vol. 2, pp 1252-1256, November-December 1993.
[12] Fardad Askarzadeh, Mohammad Heidari, Sergery Makarov , Kaveh Pahlavan, "Analysis of Effect of Micro-Metal On Ranging Error Using Finite Difference Time Domain Method", 2008 IWCMC.
[13] J. B. Keller, "Geometric Theory of Diffraction," *J. Opt. Soc. Am.*, vol. 52, pp. 116-130, 1962.
[14] R. G. Kouyoumjian and P.H. Pathak, "High frequency diffraction, focus on ray methods," *2000 IEEE Antennas and Propagation Society International Symposium*, vol. 3, p. 1638, 16-21 July 2000.
[15] Henry Bertoni, "08Diffraction.pdf" http://eeweb.poly.edu/faculty/bertoni/docs/ September 2003
[16] Henry Bertoni, "09MoreDiff.pdf" http://eeweb.poly.edu/faculty/bertoni/docs/ September 2003
[17] Kamya Yekeh Yazdandoost, Kamran Sayrafian-Pour, Wen-Bin Yang, John Hagedorn and Judith Terrill, *A Statistical Path Loss Model for Medical Implant Communication Channels*, 2009
[18] Takahiro Aoyagi, Jun-ichiTakada, Kenichi Takizawa, Norihiko Katayama, TakehikoKobayashi, Kamya Yekeh Yazdandoost, Huan-bang Li and Ryuji Kohno, *Channel models for wearable and implantable WBANs*, July 2008

[19] L. Roelens, S. Van den Bulcke, W. Joseph, G. Vermeeren and L. Martens, *Path loss model for wireless narrowband communication above flat phantom*, August 2005
[20] K. Pahlavan, Nonlinear quantization and multi-level/phase modulation and coding, IEEE Trans. Commun., (1991).
[21] K. Pahlavan, P. Krishnamurthy and J. Beneat, Wideband radio channel modeling for indoor geolocation applications, IEEE Commun. Mag., 36(4), 60-65(1998).
[22] B. Alavi, K. Pahlavan, N. Alsindi, and X. Li, "Using UWB Measurements for Statistical Analysis of the Ranging Error in Indoor Multipath Environment," accepted for publication in *International Journal of Wireless and Optical Communications (IJWOC)*, 2006.
[23] B. Alavi and K. Pahlavan, Modeling of the TOA based Distance Measurement Error Using UWB Indoor Radio Measurements, *IEEE Communication Letters*, Vol. 10, No. 4, pp: 275-277, April 2006. X. Li and K. Pahlavan, Super-resolution TOA estimation with diversity for indoor geolocation, IEEE Trans. Wireless Commun., December. 2003.
[24] X. Li Super-resolution TOA estimation with diversity.
[25] K. Yee, ``Numerical solutions of initial boundary value problems involving Maxwell's equations in isotropic media," *IEEE Transactions on Antennas and Propagation*, vol. AP-14, pp. 302-307, 1966.
[26] J. Beneat, K. Pahlavan, and P. Krishnamurthy, "Radio channel characterization for indoor and urban geolocation at different frequencies," in *Proc. IEEE PIMRC*, September 1999.
[27] B. Alavi, K. Pahlavan, X. Li, and N. Alsindi, "Indoor geolocation distance error modeling with uwb technology," in *Proceedings of IASTED 2nd International Conference on Communication and computer networks CCN 2004*, November 2004.
[28] *r networks CCN 2004*, November 2004.

Appendix .1

List of Abbreviations Used in this Chapter

TOA	Time of Arrival
RSS	Received Signal Strength
RT	Ray Tracing
FDTD	Finite Difference Time Domain
MIMO	Multiple Input Multiple Output
CDF	Cumulative Distribution Function
RMS	Root Mean Square
BPSK	Binary Phase Shift Keying
EOTD	Enhanced Observed Time Difference
GPS	Global Positioning System
LOS	Line of Sight
NLOS	Non-Line of Sight
UDP	Undetected Direct Path
POA	Phase of Arrival
UWB	Ultra Wideband
OLOS	Obstructed Line of Sight
MoM	Method of Moments
BAN	Body Area Networks
ITS	International Telecommunication Standard
NIST	National Institute of Standards and Technology
ALPS	Adaptive Lanczos-Pade Sweep
VNA	Vector Network Analyzer